Energy Proceedings
Vol 49, 2024
ISSN 2004-2965

Rapid Prediction of CO_2 Flooding Attribute Distribution in 3D Heterogeneous Reservoirs Using Fourier Neural Operator

Zepeng Yang[1], Xinwei Liao[1*], Peng Dong[2], Lingfeng Zhang[1]

1 College of Petroleum Engineering, China University of Petroleum (Beijing), Beijing, 102249, China

2 Energy Economics Institute of CNOOC, Beijing, 100013, China

(Corresponding Author: xinwei@cup.edu.cn)

ABSTRACT

During the implementation of CCUS-EOR projects, clearly defining the distribution of key attributes between injection and production wells relies on reservoir numerical simulation. However, the complex solution process of compositional models results in high computational costs for traditional numerical simulators. Deep learning surrogate models can serve as a reliable alternative to reservoir numerical simulators, significantly improving computational efficiency. This study establishes a surrogate model based on the Fourier Neural Operator (FNO) for 3D heterogeneous CO_2 displacement numerical simulation. The model predicts the distribution of pressure, CO_2 molar fraction, and oil saturation at each time step using heterogeneous porosity, permeability fields, and injection-production parameters. The research results demonstrate that the developed surrogate model can quickly and accurately predict the distribution of various attributes in the heterogeneous 3D reservoir. It can accurately capture the different displacement characteristics in the miscible and near-miscible regions during the CO_2 flooding process. Additionally, the model is able to learn from the data the differences in gas influx across perforated layers in the vertically positive rhythm and reverse rhythmic heterogeneous reservoirs, as well as the impact of gravity override on CO_2 displacement characteristics. After training, the surrogate model can achieve a 360-fold improvement in computational efficiency compared to the numerical simulator. The work in this paper has certain application prospects for engineering tasks such as rapid site selection of CO_2 injection pilot areas in heterogeneous 3D reservoirs, optimization of injection and production parameters, and determination of the migration direction of the CO_2 gas injection front.

Keywords: CO_2 flooding, numerical simulation, surrogate model, Fourier neural operator, deep learning

NONMENCLATURE

Abbreviations	
CCUS	Carbon Capture, Utilization, and Storage
EOR	Enhanced Oil Recovery
FNO	Fourier Neural Operator
Symbols	
ρ_o , ρ_w , ρ_g	Oil, water, gas phase density, kg/m^3
k_{ro} , k_{rw} , k_{rg}	Relative permeability of oil, water, gas
p_o	Oil phase pressure, MPa
N_c	Number of non-aqueous components
D	Depth, m
q_i	Injection or production rate of component i, m^3/d
S_o , S_w , S_g	Oil, water, gas phase saturation
x_i , y_i ,	Mole fraction of component i in the liquid, gas phase
z_i	Total mole fraction of component i in the hydrocarbon system
μ_o , μ_w , μ_g	Oil, water, gas viscosity, mPa·s

1. INTRODUCTION

CCUS-EOR technology can significantly increase oil recovery rates while achieving geological CO_2 storage, providing economic benefits. Given the global context of large-scale carbon emission reduction, this technology has extensive application prospects. In the application process of CO_2 flooding, understanding the distribution of underground fluids and CO_2 is crucial for formulating development technology policies. Premature gas channeling not only reduces the increase in recovery factor, but also affects the storage effectiveness, posing

This is a paper for the 16th International Conference on Applied Energy (ICAE2024), Sep. 1-5, 2024, Niigata, Japan.

great risks to personnel, equipment safety, and the environment[1–5].

Reservoir numerical simulation is a commonly used technique to determine the distribution of important properties during reservoir development. The essence of numerical simulation is to solve a system of partial differential equations that can describe the dynamics of the actual reservoir using computers. This allows us to obtain numerical distributions of important reservoir properties over time, approximating the production dynamics of the reservoir. For CO_2 flooding reservoirs, numerical simulation typically employs a compositional model. The compositional model is not based on fluid phases but starts from the composition of hydrocarbons within the reservoir, which can better reflect the changes in different components of oil, gas, and water phases during the CO_2 flooding process. Common reservoir numerical simulation software solves the model using finite difference methods, which involve complex phase equilibrium calculations and have high computational costs[6]. In recent years, with the development of deep learning, it has been widely applied in solving partial differential equations, providing new ideas for accelerating reservoir numerical simulation[7,8]. The Fourier Neural Operator (FNO) is a data-driven framework proposed by Li[9] for solving partial differential equations. This method uses neural networks to learn the mapping between infinite-dimensional function spaces, enabling the transfer of solution strategies. Existing research results have shown that FNO can accurately solve underground multiphase flow problems while demonstrating excellent generalization capabilities[10-17].

In this study, the Fourier neural operator is applied to the numerical simulation problem of 3D heterogeneous CO_2 flooding reservoirs. Based on the FNO framework, a surrogate model for reservoir numerical simulation is established to solve the field diagram problem of pressure, CO_2 mole fraction and oil saturation at each time step in the CO_2 flooding reservoir under heterogeneous reservoirs and different injection and production parameters.

2. PROBLEM SETTING

2.1 Governing equation

The governing equations for the CO_2 flooding compositional model assume the presence of three phases in the reservoir: oil, gas, and water, with N_c components. Each component can exist and move in multiple phases, while undergoing mass exchange between different phases. The governing equation is represented by Equation (1).

$$\begin{aligned}&\nabla\cdot\left[\frac{k\rho_w k_{rw}}{\mu_w}\nabla(p_o-\rho_w gD)\right]+q_w=\frac{\partial}{\partial t}\left(\varphi\rho_w S_w\right)\\&\nabla\cdot\left[\frac{k\rho_o k_{ro}}{\mu_o}x_i\nabla(p_o-\rho_o gD)\right]+\nabla\cdot\left[\frac{k\rho_g k_{rg}}{\mu_o}y_i\nabla(p_o+p_{cgo}-\rho_g gD)\right]+q_i\\&=\frac{\partial}{\partial t}\left(\varphi(\rho_o S_o+\rho_g S_g)z_i\right)(i=1,2,\cdots,N_c-1)\end{aligned}\quad(1)$$

2.2 Numerical simulation setting

In this study, a 3D heterogeneous five-spot well pattern CO_2 flooding compositional model was established using the CMG reservoir simulator. The model consisted of a grid with dimensions of 21x21x5 cells in the X, Y, and Z directions, respectively, with a horizontal grid spacing of 20m and a vertical grid spacing of 2m. An injection well was positioned at the center of the reservoir, while production wells were placed at the four corners. The distance between the injection well and the production wells was 300m, with all wells perforated within the vertical extent of the reservoir. The original formation pressure of the reservoir was 22MPa, and the original oil saturation was 0.8.

2.3 Variable sampling scheme

By varying the reservoir heterogeneity porosity field, the heterogeneity permeability field, gas injection rate, and the bottomhole flowing pressure in the production well, we aim to investigate the temporal variations of reservoir pressure, CO_2 mole fraction, and oil saturation distribution during the CO_2 flooding process under different reservoir and injection-production parameters.

The heterogeneity field is generated based on a Gaussian covariance model[18], as shown in Equation (2). Using the covariance model, a spatial random field is generated using the randomization method proposed by Heße[19].

$$\gamma(r)=\sigma^2\left(1-\exp\left(-\left(s\cdot\frac{r}{\ell}\right)^2\right)\right)+n \quad(2)$$

Where r is the (isotropic) lag distance, l is the main correlation length, s is a rescaling factor to adjust model representation, σ^2 is the variance, and n is the nugget value.

Furthermore, we investigate the impact of intra-layer heterogeneity on the performance of CO_2 flooding. We set the permeability contrast ratio to 27 and consider two types of moderately heterogeneous reservoirs: positive rhythm and reverse rhythm. Figure 1 shows two types of random heterogeneous permeability and porosity field maps generated using the above model.

The distribution range of each variable is shown in Table 1.

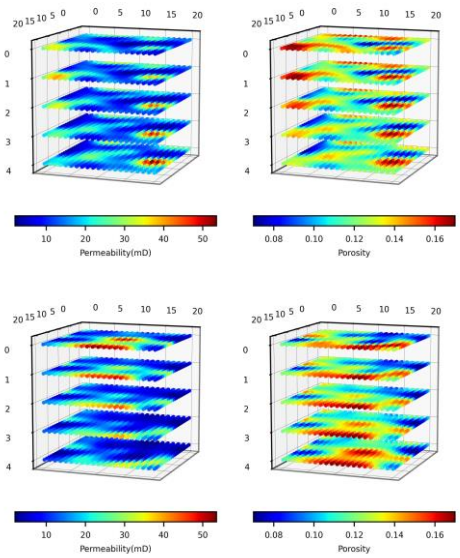

Fig.1 Permeability and porosity distribution diagrams of heterogeneous reservoirs with positive rhythm (top) and reverse rhythm (bottom)

Table 1 The value ranges of each variable

Variable	Ranges
reservoir gas injection rate, m^3/d	20-30
production pressure differential, MPa	2-4
porosity field	0.07-0.17
permeability field, mD	1.98-53.48

Using the Latin Hypercube Sampling method [20], we generated 1000 diverse cases of heterogeneous fields and injection-production parameters. We simulated CO_2 flooding for 60 months, with each time step representing a period of 3 months. The GEM compositional simulator was utilized to compute the numerical model, resulting in a time series dataset comprising pressure, CO_2 mole fraction, and oil saturation distributions for 20 time steps. The dataset was partitioned into training, validation, and testing sets in an 8:1:1 ratio.

3. METHODOLOGY

3.1 FNO Architecture

For a nonlinear mapping $\mathcal{F}^{\dagger}:\mathcal{A}\to\mathcal{U}$, where $\mathcal{A}$ is the input function space and $\mathcal{U}$ is the output function space, assuming we have observed values $\{a_j,u_j\}_{j=1}^{N}$, the neural operator constructs an operator $\mathcal{F}_\theta$ using a neural network for certain finite-dimensional parameter space θ. The goal is to learn an approximation of $\mathcal{F}^{\dagger}$ by minimizing the cost function, as shown in Equation (3). In this paper, the input and output are functions defined on a 4D domain based on the corresponding function spaces $\mathcal{A}=\mathcal{U}=L^{\infty}(D)$, where the 4D domain refers to a 3D reservoir with time.

$$\min_{\theta}\mathbb{E}_{a\sim\mu}[C(\mathcal{F}_\theta(a),\mathcal{F}^{\dagger}(a))] \tag{3}$$

The complete architecture of the FNO employed in this study is illustrated in Figure 2. Following the input of the heterogeneous reservoir and injection-production parameters, they are passed through a fully connected layer P to elevate to a high-dimensional channel space. Subsequently, they undergo four iterations of Fourier layers from to. Finally, they are transformed to the dimension of the output solution via a fully connected layer, representing the distribution of important properties at each time step. The iterative architecture of the FNO described above is represented by Equation (4).

$$\begin{aligned} v_0(x)&=P\big(a(x)\big)\\ v_{t+1}(x)&=\sigma\Big(Wv_t(x)+\big(\mathcal{K}(a;\phi)v_t\big)(x)\Big),\forall x\in D\\ u(x)&=Qv_T(x)+q \end{aligned} \tag{4}$$

Within each Fourier layer, the input $v(x)$ is first transformed to the Fourier domain using the Fourier transform $\mathcal{F}$. Then, a linear transformation R is applied to filter out high-frequency modes, which enhances the network's generalization capability and speed. Next, the result is transformed back to the original space using the inverse Fourier transform $\mathcal{F}^{-1}$. Meanwhile, the input

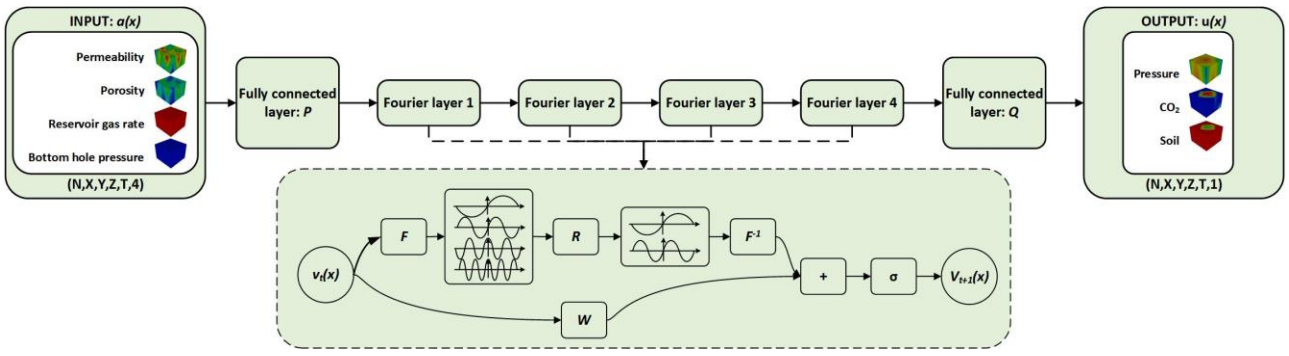

Fig. 2 Full architecture of FNO

$v(x)$ is also linearly transformed by W. The two branches are then summed and passed through an activation function for nonlinear transformation.

3.2 Loss function design and training

We obtain the solution in the 4D spatiotemporal domain based on the FNO-4D framework. The model input is a 6D tensor $\{N,X,Y,Z,T,4\}$, which includes the heterogeneous porosity field, heterogeneous permeability field, gas injection rate, and production well bottom-hole pressure. The model output is a 6D tensor $\{N,X,Y,Z,T,1\}$, which contains the distribution of different properties at different time steps, where N is the number of samples, X, Y, and Z are the grid numbers in different directions, and T is the number of time steps to be predicted.

To improve the accuracy and convergence speed of the surrogate model predictions, the neural network parameters are optimized using the relative loss during the training process. The loss function is defined as shown in Equation (5), where the first part is the data-driven loss function L_{data}, and the second part is the loss function $L_{partial}$ that considers the gradient relationships of the properties in the X, Y, Z, and T directions in the governing equations. Using the L_2 loss between the true values and predicted values, divided by the L_2 norm of the true values, can measure the prediction error relative to the overall range of the true values, making the loss function more stable and having a certain regularization effect [10,11].

$$
\begin{aligned}
&Loss = L_{data} + L_{partial} \\
&L_{data} = \frac{\|u-\hat{u}\|_2}{\|u\|_2} \\
&L_{partial} = \lambda_x \frac{\|d_u/d_x - d_{\hat{u}}/d_x\|_2}{\|d_u/d_x\|_2} + \lambda_y \frac{\|d_u/d_y - d_{\hat{u}}/d_y\|_2}{\|d_u/d_y\|_2} + \\
&\lambda_z \frac{\|d_u/d_y - d_{\hat{u}}/d_y\|_2}{\|d_u/d_y\|_2} + \lambda_t \frac{\|d_u/d_t - d_{\hat{u}}/d_t\|_2}{\|d_u/d_t\|_2}
\end{aligned} \tag{5}
$$

Where u is the true values, $\hat{u}$ is the predicted values, d_u/d_x, $d_{\hat{u}}/d_x$, d_u/d_y, $d_{\hat{u}}/d_y$, d_u/d_z, $d_{\hat{u}}/d_z$, d_u/d_t, $d_{\hat{u}}/d_t$ represent the first-order derivatives of true and predicted values in the X, Y, Z, and T directions, respectively. λ_x, λ_y, λ_z and λ_t are hyperparameters.

The numerical model and surrogate model in this study were run on hardware environment consisting of Intel Core i7-12700 and NVIDIA GeForce GTX 3090 GPU. During the training process, the Adam optimizer was utilized along with a cosine annealing learning rate schedule to adjust the model parameters. The initial learning rate was set to 0.001, and mini-batch training was employed with a batch size of 5. The training was conducted for 100 epochs.

4. RESULTS

Figure 3 presents the training and validation set relative loss curves for pressure, CO_2 mole fraction, and oil saturation distribution based on the FNO framework. The R^2 scores for the test set at all time steps are 0.967, 0.989, and 0.973, respectively.

To provide a more intuitive representation of the error distribution in the predictions of the surrogate model, taking a positive rhythm heterogeneous reservoir and a reverse rhythm heterogeneous reservoir in the test set as examples, the simulator calculation results, surrogate model prediction results and residuals of different attributes at the last time step are plotted, the positive rhythm reservoir is shown in Figure 4, and the reverse rhythm reservoir is shown in Figure 5.

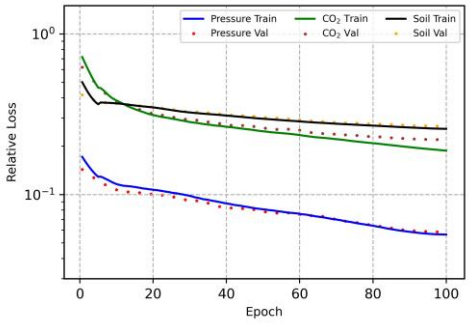

Fig. 3 Relative loss of training set and validation set for each attribute

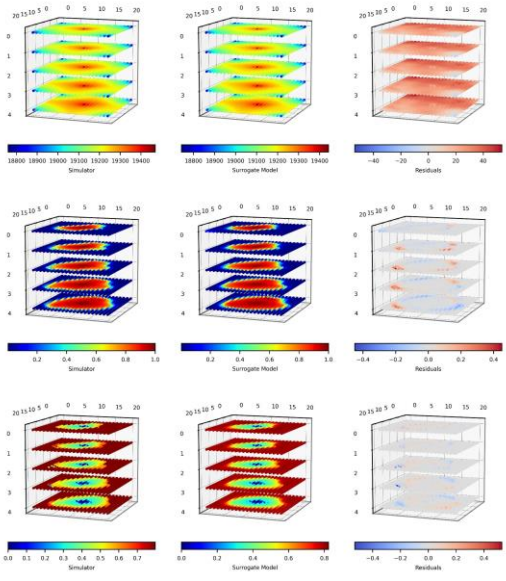

Fig.4 Simulator calculation results, surrogate model prediction results and residuals of positive rhythm reservoir pressure (top), CO_2 mole fraction (middle) and oil saturation (bottom)

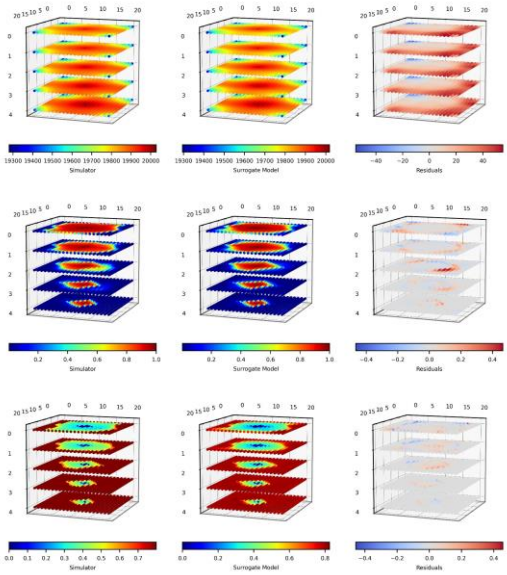

Fig.5 Simulator calculation results, surrogate model prediction results and residuals of reverse rhythm reservoir pressure (top), CO_2 mole fraction (middle) and oil saturation (bottom)

5. DISCUSSION

The relative loss of the model decreases in a similar trend on both the training and validation sets, indicating that our designed loss function has a good regularization effect and avoids overfitting. Through testing, it has been found that adding the first-order derivative loss to the loss function can make the distribution of predicted values smoother. Compared to using only the L_{data} loss, the inclusion of the first-order derivative loss reduces the presence of outliers and makes the distribution of predicted values more consistent with physical meaning. The R^2 score of the model on the validation set is close to 1, indicating that the model based on FNO can accurately predict the distribution of properties in the 4D domain and exhibits good generalization ability.

By comparing the simulator calculation results and surrogate model predictions for the positive rhythm and reverse rhythm heterogeneous reservoir cases at the last time step, it can be observed that the error in pressure prediction is mainly concentrated around the production well bottomhole, where the pressure changes fluctuate significantly, posing certain challenges for the model's accurate prediction. For the predictions of CO_2 mole fraction distribution and oil saturation distribution, the errors are primarily concentrated in the transition zone where the oil and gas interact with the CO_2 front. In this region, the phase behavior is highly complex due to the large number of pseudo-components and the critical state of temperature and pressure, where the CO_2 extraction of light oil components makes it difficult for the surrogate model to learn the simulator's phase behavior rules.

The fluid model used in this study has a minimum miscibility pressure of approximately 25 MPa. All the original reservoir pressures in the cases are 22 MPa, under which conditions the region near the injection well bottomhole can reach miscible displacement, while the areas away from the injection and production well bottomholes are in the near-miscible displacement regime. The distribution of the oil saturation prediction errors indicates that the surrogate model has accurately learned this characteristic.

There is no significant difference in the prediction accuracy of our model between positive rhythm and reverse rhythmic heterogeneous reservoirs, indicating that the model accurately learns the differences in gas intake at different perforation positions under the influence of rhythm. At the same time, the characteristics of aggravated CO_2 gravity segregation in reverse rhythmic reservoirs can also be captured by the model.

The surrogate model takes approximately 209 seconds on average for each training epoch, while after training, it can predict a batch in just 0.005 seconds. In contrast, the numerical simulator takes an average of 1.8 seconds to compute a single case. Additionally, the surrogate model is capable of parallel computing, and the increase in computational cost with an increase in the number of cases is much smaller compared to the numerical simulator. Therefore, the surrogate model can significantly improve the efficiency of solving engineering problems that require a large number of repeated model computations.

6. CONCLUSIONS

This study establishes a 3D heterogeneous reservoir five-spot well pattern CO_2 flooding numerical simulation surrogate model based on FNO. The model predicts pressure, CO_2 molar fraction, and oil saturation distribution using heterogeneous permeability, porosity field, and injection-production parameters. Results demonstrate that the surrogate model exhibits high prediction accuracy and good generalization ability. Post-training, the surrogate model achieves a 360-fold increase in prediction speed compared to the numerical simulator, while also supporting parallel computing, thus significantly reducing computational costs in engineering problems requiring extensive model computations.

Furthermore, the surrogate model we established is based on the 4D domain for prediction, which can

accurately capture the differences in the distribution of various attributes in different perforation layers under the influence of rhythms and gravity, which greatly increases the applicability of the model. The work in this paper can assist engineers in making quick decisions and has certain application prospects in engineering tasks such as rapid site selection of CO_2 injection pilot areas in heterogeneous 3D reservoirs, optimization of injection-production parameters, and determination of the migration direction of the CO_2 gas injection front.

ACKNOWLEDGEMENT

The authors sincerely thank the colleagues at State Key Laboratory of Petroleum Resources, and CMG-CUP Joint Numerical Reservoir Simulation Laboratory for their help.

REFERENCE

[1] Chen S, Liu J, Zhang Q, et al. A critical review on deployment planning and risk analysis of carbon capture, utilization, and storage (CCUS) toward carbon neutrality[J]. Renewable and Sustainable Energy Reviews, 2022, 167: 112537.

[2] Storrs K, Lyhne I, Drustrup R. A comprehensive framework for feasibility of CCUS deployment: A meta-review of literature on factors impacting CCUS deployment[J]. International Journal of Greenhouse Gas Control, 2023, 125: 103878.

[3] Davoodi S, Al-Shargabi M, Wood D A, et al. Review of technological progress in carbon dioxide capture, storage, and utilization[J]. GAS SCIENCE AND ENGINEERING, 2023, 117: 205070.

[4] Kuuskraa V A, Godec M L, Dipietro P. CO_2 Utilization from "Next Generation" CO_2 Enhanced Oil Recovery Technology[C]//Dixon T, Yamaji K. GHGT-11: Vol. 37. Amsterdam: Elsevier Science Bv, 2013: 6854-6866.

[5] Hill L B, Li X, Wei N. CO_2-EOR in China: A comparative review[J]. INTERNATIONAL JOURNAL OF GREENHOUSE GAS CONTROL, 2020, 103: 103173.

[6] Aziz K, Settari A. Petroleum Reservoir Simulation[J]. Applied Science Publishers, 1979.

[7] Lu L, Jin P, Karniadakis G E. DeepONet: Learning nonlinear operators for identifying differential equations based on the universal approximation theorem of operators[J]. Nature Machine Intelligence, 2021, 3(3): 218-229.

[8] Chen X, Zhang K, Ji Z, et al. Progress and Challenges of Integrated Machine Learning and Traditional Numerical Algorithms: Taking Reservoir Numerical Simulation as an Example[J]. Mathematics, 2023, 11(21): 4418.

[9] Li Z, Kovachki N, Azizzadenesheli K, et al. Fourier Neural Operator for Parametric Partial Differential Equations[EB/OL]. (2021-05-17)[2023-09-08]. http://arxiv.org/abs/2010.08895v3.

[10] Wen G, Li Z, Azizzadenesheli K, et al. U-FNO—An enhanced Fourier neural operator-based deep-learning model for multiphase flow[J]. Advances in Water Resources, 2022, 163: 104180.

[11] Liu J, Jing H, Pan H. New Fast Simulation of 4D (x, y, z, t) CO_2 EOR by Fourier Neural Operator Based Deep Learning Method[C]//SPE Reservoir Simulation Conference. OnePetro, 2023.

[12] Choubineh A, Chen J, Wood D A, et al. Fourier Neural Operator for Fluid Flow in Small-Shape 2D Simulated Porous Media Dataset[J]. Algorithms, 2023, 16(1): 24.

[13] Witte P A, Konuk T, Skjetne E, et al. Fast CO_2 saturation simulations on large-scale geomodels with artificial intelligence-based Wavelet Neural Operators[J]. International Journal of Greenhouse Gas Control, 2023, 126: 103880.

[14] Grady T J, Khan R, Louboutin M, et al. Model-parallel Fourier neural operators as learned surrogates for large-scale parametric PDEs[J]. Computers & Geosciences, 2023, 178: 105402.

[15] Tang H, Kong Q, Morris J P. Multi-fidelity Fourier Neural Operator for Fast Modeling of Large-Scale Geological Carbon Storage[M]. arXiv, 2023.

[16] Wen G, Li Z, Long Q, et al. Real-time high-resolution CO_2 geological storage prediction using nested Fourier neural operators[J]. Energy & Environmental Science, 2023, 16(4): 1732-1741.

[17] Tariq Z, Yan B, Sun S. Physics Informed Surrogate Model Development in Predicting Dynamic Temporal and Spatial Variations During CO_2 Injection into Deep Saline Aquifers[C]//SPE Reservoir Characterisation and Simulation Conference and Exhibition. OnePetro, 2023.

[18] Webster R, Oliver M A. Characterizing Spatial Processes:The Covariance and Variogram[M]//Geosta tistics for Environmental Scientists. John Wiley & S ons, Ltd, 2007: 47-76.

[19] Heße F, Prykhodko V, Schlüter S, et al. Generating random fields with a truncated power-law variogram: A comparison of several numerical methods[J]. Environmental Modelling & Software, 2014, 55: 32-48.

[20] Helton J C, Davis F J. Latin hypercube sampling and the propagation of uncertainty in analyses of complex systems[J]. Reliability Engineering & System Safety, 2003, 81(1): 23-69.